

Synthesis and characterization of $Zn_xMn_{(1-x)}Fe_2O_4$

Nguyen Le My Linh^{1*}, Do Mai Nguyen²

¹University of Education, Hue University, 34 Le Loi St., Hue City, Vietnam

²University of Sciences, Hue University, 77 Nguyen Hue St., Hue City, Vietnam

* Correspondence to Nguyen Le My Linh <nlmlinh@hueuni.edu.vn>

(Received: 21 November 2024; Revised: 23 December 2024; Accepted: 30 December 2024)

Abstract. $Zn_xMn_{(1-x)}Fe_2O_4$ nanoparticles were successfully prepared in the isopropanol solvent with the hydrothermal method and the hydrothermal method combined with impregnation. The characterization of the samples by using X-ray diffraction (XRD), scanning electron microscopy (SEM), Fourier Transform Infrared (FTIR), and surface area analysis (BET) was conducted. The samples synthesized with the hydrothermal method had a phase composition of franklinite $(Zn,Mn,Fe)(Fe,Mn)_2O_4$. Meanwhile, the samples synthesized with the hydrothermal method combined with impregnation had the main phase composition of $Zn_xMn_{(1-x)}Fe_2O_4$. The $Zn_{0.8}Mn_{0.2}Fe_2O_4$ ($ZnFe_2O_4/MnSO_4$ molar ratio = 4:1) sample exhibited the highest degree of structural order, with a BET surface area of 25.7 m²/g.

Keywords: $Zn_xMn_{(1-x)}Fe_2O_4$, hydrothermal method, nanomaterial

1 Introduction

In recent years, the development of hybrid structures based on spinel ferrite nanomaterials (SFNs) [1–7] has garnered significant attention from researchers because of the fascinating physicochemical properties of SFNs (e.g., optical, electrical, and magnetic properties), as well as their high chemical stability and ease of functionalization. These materials have found applications in catalysts, gas sensors, rechargeable lithium batteries, information storage systems, magnetic bulk cores, adsorbents, etc. [1–4]. Jun Wang et al. [8] synthesized $Zn_xMn_{(1-x)}Fe_2O_4$ nanoparticles coated with SiO_2 , and the material exhibits enhanced magnetic properties. The core-shell $Zn_xMn_{(1-x)}Fe_2O_4/SiO_2$ nanoparticles (average diameter of approximately 80 nm) were prepared through the hydrolysis of tetraethyl orthosilicate (TEOS) in ethanol-water solutions in the presence of $Zn_xMn_{(1-x)}Fe_2O_4$ nanoparticles (average diameter of approximately 10 nm) synthesized via

the hydrothermal method. The magnetic properties of the material were evaluated by using a vibrating sample magnetometer (VSM), and the results indicated improved room-temperature magnetism compared with materials synthesized with the co-precipitation method. A study by Granone et al. [9] focused on the synthesis of silica nanoparticles with a magnetic $ZnFe_2O_4$ core in a water-oil emulsion system, which allows control over the size, shape, and spacing of the nanoparticles. Initially, a water-based magnetic fluid was prepared from zinc ferrite nanoparticles with sizes ranging from 4 to 6 nm and synthesized with a soft chemical method. Chemical analysis revealed asymmetric zinc ferrite nanoparticles with an estimated formula of $Zn_{0.87}Fe_{2.09}X_{0.04}O_4$ (X represents substitutional sites). The silica nanoparticles obtained (40–60 nm) with zinc ferrite cores (4–6 nm) were characterized by using X-ray diffraction, electron microscopy, and magnetic saturation techniques.

Yao Li et al. [10] synthesized Ni-Zn ferrite powders using the self-propagating high-temperature synthesis (SHS) method. The effect of temperature (T_c), a key parameter in the SHS process, on the particle size, phase composition, and magnetic properties was also investigated. The results show that the particle size increased with higher T_c , and the saturation magnetization (M_s) values similarly increased with rising T_c . Compared with other methods, the SHS method provided $Ni_{0.35}Zn_{0.65}Fe_2O_4$ ferrite powders with enhanced magnetic properties at 1,000 °C.

In Vietnam, no publications on $Zn_xMn_{(1-x)}Fe_2O_4$ nanomaterials have been identified. In this study, $Zn_xMn_{(1-x)}Fe_2O_4$ materials were synthesized with two different methods (hydrothermal method and hydrothermal method combined with impregnation), and their phase composition and structure were thoroughly investigated.

2 Method

2.1 Chemicals

$Fe_2(SO_4)_3 \cdot 9H_2O$, $ZnSO_4 \cdot 7H_2O$, $MnSO_4 \cdot H_2O$ (Guangdong, China, 99%), NaOH (Xilong, China), and Isopropanol (Guangdong, China) were used in this study.

2.2 Synthesis of $Zn_xMn_{(1-x)}Fe_2O_4$

The $Zn_xMn_{(1-x)}Fe_2O_4$ material was synthesized with two methods.

Method 1 (hydrothermal method): A solution was prepared by dissolving 20 mL of isopropanol in 40 mL of distilled water and stirred with a magnetic stirrer at 500 rpm until the alcohol was fully dissolved. Subsequently, x grams of $ZnSO_4 \cdot 7H_2O$, y grams of $Fe_2(SO_4)_3 \cdot xH_2O$, and z grams of $MnSO_4 \cdot H_2O$ were added to the solution, and stirring was continued until the solids were completely dissolved. A volume of 40 mL of 2 M NaOH was then gradually added dropwise to the

mixture while stirring continuously for one hour. The resulting mixture was transferred into a Teflon-lined autoclave, sealed tightly, and placed in an oven at 120 °C for 12 or 24 hours. After the reaction, the autoclave was allowed to cool naturally to ambient temperature. The obtained precipitate was filtered and washed with distilled water until the filtrate reached a pH of approximately 7. The product was dried at 80 °C and then calcined at 500 °C for four hours. Table 1 presents the notations of the synthesized samples with varying Zn/Fe/Mn molar ratios.

Table 1. Synthesized samples denoted based on different Zn/Fe/Mn molar ratios

Sample	Zn/Fe/Mn ratio (n/n/n)	Hydrolysis time (hour)
M1	2:1:8	12
M2	2:1:8	24
M3	5:1:5	24
M4	8:1:2	24

In this method, the effect of NaOH concentration was also investigated. The Zn/Mn/Fe molar ratio was fixed at 8:1:2, while the NaOH concentrations were varied at 0.5, 1.0, 2.0, and 3.0 M.

Method 2 (Thermal hydrolysis combined with impregnation): The $Zn_xMn_{(1-x)}Fe_2O_4$ material was synthesized in 2 steps.

Step 1: The synthesis of $ZnFe_2O_4$ spinel nanoparticles was carried out, according to the method described in reference [11], similar to the synthesis of $Zn_xMn_{(1-x)}Fe_2O_4$ materials, except that manganese-containing $MnSO_4 \cdot H_2O$ was excluded from the initial solution. The synthesized samples were designated as M5 to M9, where M5 represents $ZnFe_2O_4$ without calcination, and M9 represents $ZnFe_2O_4$ calcined at 500 °C for four hours.

Step 2: 20 mL of 2 M NaOH was gradually added dropwise to a mixture containing *a* grams of ZnFe₂O₄ (sample M5 or M9), *b* grams of MnSO₄·H₂O, and 20 mL of distilled water. The mixture was then stirred for two hours. The resulting product was dried at 80 °C and characterized by using XRD. Table 2 presents the notations of the synthesized samples under various conditions.

Table 2. Synthesized samples were under various conditions

Sample	ZnFe ₂ O ₄ /MnSO ₄ (<i>n/n</i>) ratio	V _{NaOH} (mL)
M5	The ZnFe ₂ O ₄ sample synthesized in step 1, uncalcined	
M6	1:2	20
M7	2:1	20
M8	4:1	20
M9	The ZnFe ₂ O ₄ sample synthesized in step 1, calcined at 500 °C	
M10	1:2	20
M11	2:1	20
M12	4:1	20

3 Results and discussion

3.1 Synthesis of spinel nanomaterials Zn_xMn_(1-x)Fe₂O₄ with Method 1

a. Effect of different Zn/Mn/Fe molar ratios

The Zn_xMn_(1-x)Fe₂O₄ material was synthesized at different Zn/Mn/Fe molar ratios with Method 1, as described in Section 2.3. The XRD patterns of these samples are presented in Fig. 1.

It can be seen that the XRD patterns of the synthesized samples exhibit characteristic peaks corresponding to the cubic crystal phase of franklinite (Zn,Mn,Fe)(Fe,Mn)₂O₄ at 2θ around 30.00, 35.42, 58.48, and 61.52° (JCPDS 10-0467). In the franklinite structure, Fe and Mn exist in two forms, namely Fe²⁺ and Fe³⁺, and Mn²⁺ and Mn³⁺.

This synthesis method enables Zn²⁺ in the tetrahedral sites to be substituted by Mn²⁺ and Fe²⁺ cations, while Fe³⁺ in the octahedral sites is partially replaced by Mn³⁺ cations. When the synthesis was performed at a Zn/Mn/Fe molar ratio of 2:1:8 for 12 hours (sample M1), the (Zn,Mn,Fe)(Fe,Mn)₂O₄ crystal phase formed with a low structural order. Extending the reaction time to 24 hours with the same molar ratio (sample M2) resulted in an improved structural order. When the Zn/Mn/Fe ratios were from 2:1:8 (M2) to 8:1:2 (M4), the characteristic peaks of the (Zn,Mn,Fe)(Fe,Mn)₂O₄ crystal phase became sharper, indicating an increasingly ordered structure. Additionally, no peaks corresponding to other crystal phases were observed in the XRD patterns, confirming the purity of the synthesized material. The Zn/Mn/Fe molar ratio of 8:1:2 was selected for further studies.

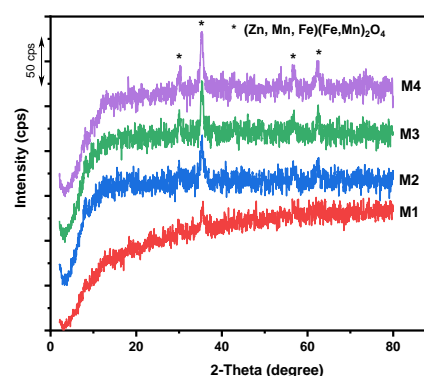


Fig. 1. XRD diagram of the M1, M2, M3, and M4 samples

b. Effect of various NaOH concentrations

The XRD patterns of the samples with molar ratio Zn/Mn/Fe = 8:1:2 (M4) synthesized at different NaOH concentrations are depicted in Fig. 2.

Fig. 2 shows that all the XRD patterns of the synthesized samples exhibit characteristic peaks corresponding to the cubic phase of franklinite (Zn,Mn,Fe)(Fe,Mn)₂O₄ (JCPDS 10-0467). At this Zn/Mn/Fe molar ratio (2:1:8), varying NaOH concentrations from 0.5 M to 3 M does not change the shape of the characteristic peaks of the

(Zn,Mn,Fe)(Fe,Mn)₂O₄ crystal, indicating that the structural order of the material is not significantly dependent on the NaOH concentration within this concentration range.

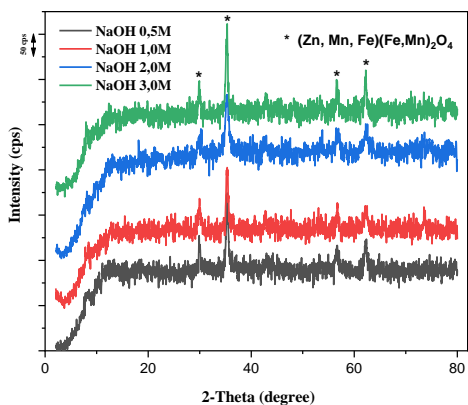


Fig. 2. XRD diagram of some synthesized samples at various NaOH concentrations

3.2 Synthesis of spinel nanomaterial Zn_xMn_(1-x)Fe₂O₄ with Method 2

The Zn_xMn_(1-x)Fe₂O₄ materials synthesized using method 2 with the different ZnFe₂O₄/MnSO₄ molar ratios were characterized with XRD, as shown in Fig. 3.

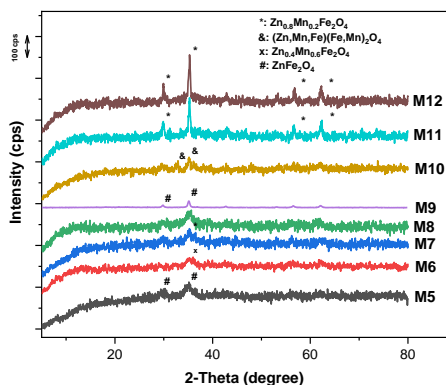


Fig. 3. XRD spectra of Zn_xMn_(1-x)Fe₂O₄ materials synthesized using method 2

The figure demonstrates that sample M5 exhibits characteristic peaks corresponding to the ZnFe₂O₄ crystal phase (JCPDS 22-1012) [11]. This sample was synthesized in step 1 without calcination. Sample M6 (synthesized by

introducing Mn²⁺ ions into the ZnFe₂O₄ crystal lattice with a ZnFe₂O₄/MnSO₄ molar ratio of 1:2 and adding NaOH during the stirring stage) displayed characteristic peaks of the Zn_{0.4}Mn_{0.6}Fe₂O₄ crystal phase, indicating that Mn²⁺ ions partially replaced Zn²⁺ in the tetrahedral site. When the ZnFe₂O₄/MnSO₄ molar ratio was adjusted to 2:1 (sample M7) and 4:1 (sample M8), the substitution of Zn²⁺ with Mn²⁺ in the tetrahedral site was reduced, resulting in the formation of the Zn_{0.8}Mn_{0.2}Fe₂O₄ crystal phase. Therefore, variations in the ZnFe₂O₄/MnSO₄ molar ratio lead to differences in the extent of Mn²⁺ substitution for Zn²⁺ in the tetrahedral site. Sample M9 shows characteristic peaks corresponding to the ZnFe₂O₄ crystal phase. This sample was synthesized in step 1 and calcined at 500 °C for 4 hours. When Mn²⁺ ions are introduced into the ZnFe₂O₄ crystal structure at a ZnFe₂O₄/MnSO₄ molar ratio of 1:2, the resulting product displays characteristic peaks of franklinite. In contrast, at a molar ratio of 4:1 (sample M12), the synthesized material has characteristic peaks of the Zn_{0.8}Mn_{0.2}Fe₂O₄ crystal phase. Among the investigated samples, M12 demonstrates the sharpest peaks with the highest intensity, indicating the highest degree of structural order. Furthermore, no diffraction peaks corresponding to other crystal phases were observed, confirming the purity of the synthesized material.

The analysis results indicate that when the materials are synthesized with Method 1, a portion of Fe³⁺ ions in the octahedral site is replaced by Mn³⁺ ions. In contrast, with Method 2, ZnFe₂O₄ is first synthesized, followed by introducing Mn²⁺ ions into the crystal lattice. The resulting product meets the desired outcome, i.e., only a partial substitution of Zn²⁺ ions with Mn²⁺ ions. The samples synthesized with ZnFe₂O₄/MnSO₄ molar ratios of 4:1 and 2:1 exhibit superior properties compared with those

synthesized at the molar ratio of 1:2. Furthermore, if the $ZnFe_2O_4$ sample synthesized in the first step is calcined at 500 °C (sample M12), the resulting $Zn_{0.8}Mn_{0.2}Fe_2O_4$ exhibits the highest degree of structural order. Therefore, sample M12 meets the desired phase structure and will be further investigated.

3.3 Characterization of the M12 sample

Sample M12 was characterized by using EDX spectroscopy (Fig. 4), infrared (IR) spectroscopy (Fig. 5), scanning electron microscopy (SEM) (Fig. 6), and nitrogen adsorption-desorption isotherms (BET) (Fig. 7).

The presence of elements in the $Zn_{0.8}Mn_{0.2}Fe_2O_4$ material was examined by using the EDX method. The EDX results confirm the presence of the Zn, Mn, Fe and O atoms (Fig. 4).

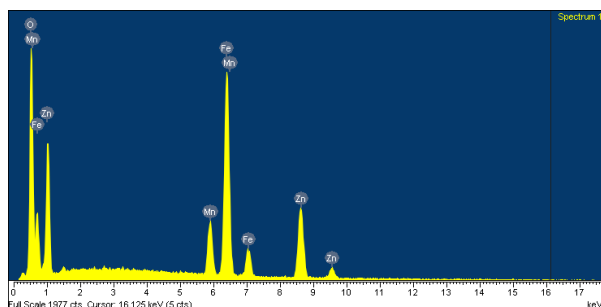


Fig. 4. EDX spectrum of M12 sample

The chemical composition of the M12 sample is summarized in Table 3.

Table 3. Element composition of $Zn_{0.8}Mn_{0.2}Fe_2O_4$ sample

Weight % O	Weight % Zn	Weight % Mn	Weight % Fe	Zn/Mn/Fe atomic ratio
29.85	29.23	5.24	35.74	4:1:5

The EDX result indicates that the Zn/Mn/Fe atomic ratio of the M12 sample is 4:1:5.

The FTIR spectrum of the M12 sample (Fig. 5) exhibits a peak at 3439.1 cm^{-1} , corresponding to the O–H stretching vibration of physically adsorbed

water, and a peak at 1629.9 cm^{-1} characterises the bending vibration δ_{H-O-H} . The peak at 1400.3 cm^{-1} is attributed to the bending vibration of the C–H bond in the CH_3 group [11], while the peak at 1163.1 cm^{-1} is assigned to C–O stretching [12], indicating the presence of residual isopropanol in the sample. The peaks corresponding to M–O vibrations (M = Fe, Mn, Zn) are observed in the range of 364.6–543.4 cm^{-1} [13].

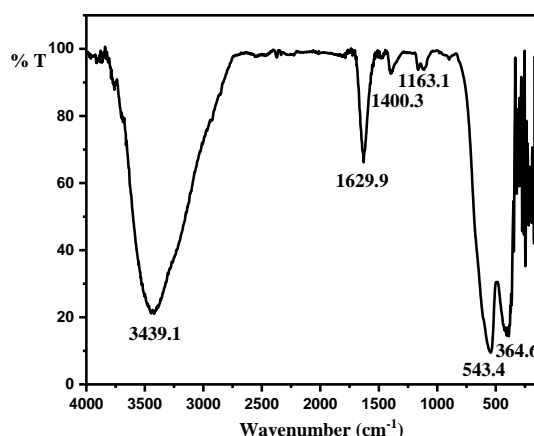


Fig. 5. FTIR spectra of M12 sample

Fig. 6 illustrates the SEM image of the M12 sample.

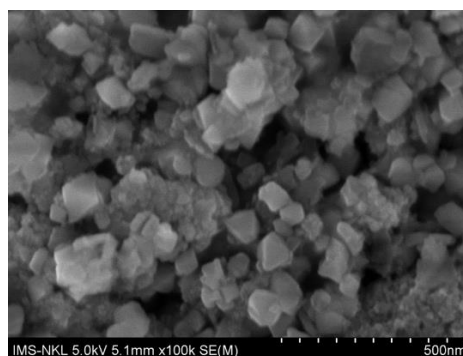


Fig. 6. SEM image of M12 sample

The image shows nanoparticles with varying sizes. Smaller particles are observed within voids formed among larger particles, which appear to result from the fragmentation of these particles.

The surface properties and pore structure of sample M12 were investigated by using N₂ adsorption-desorption measurement at 77 K. Fig. 7 presents the N₂ adsorption-desorption isotherm of this sample.

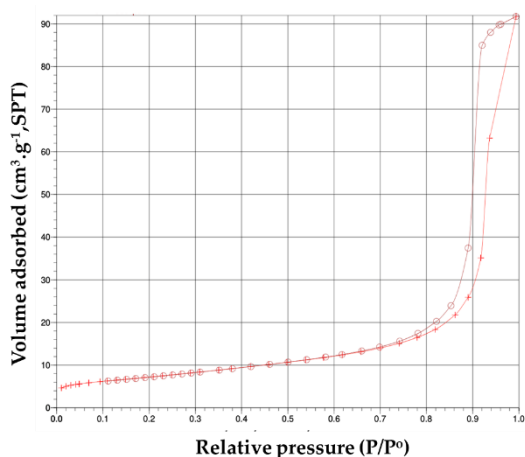


Fig. 7. Nitrogen adsorption-desorption isotherm of sample M12

From Fig. 7, it is obvious that this isotherm belongs to Type IV, according to the IUPAC classification. The presence of a hysteresis loop in the relative pressure region P/P° of 0.7–1.0 is likely associated with voids formed among adjacent nanoparticles. The BET (Brunauer-Emmett-Teller) equation provides a specific surface area of 25.7 m²/g.

4 Conclusion

The spinel nanomaterial Zn_xMn_(1-x)Fe₂O₄ was synthesized in isopropanol with two different methods. The sample synthesized with Method 1 exhibited a franklinite (Zn,Mn,Fe)(Fe,Mn)₂O₄ phase composition. In contrast, samples synthesized with Method 2 predominantly consisted of the Zn_xMn_(1-x)Fe₂O₄ phase. Among the samples synthesized with Method 2, the Zn_{0.8}Mn_{0.2}Fe₂O₄ (ZnFe₂O₄/MnSO₄ molar ratio = 4:1) illustrated the highest degree of structural order, with a BET surface area of 25.7 m²/g.

Acknowledgment

Do Mai Nguyen was funded by the Master and PhD. Scholarship Programme of Vingroup Innovation Foundation (VINIF), code VINIF.2024.TS.032

Reference

1. Ranjbaran A, Abbasi F, Khazaei M, Moosavi-Zareb AR. Synthesis, characterization and application of ZnFe₂O₄ nanoparticles as a heterogeneous ditopic catalyst for the synthesis of pyrano[2,3-d]pyrimidines. *RSC Advances*. 2015;5(18):13643-13647.
2. Yang X, Ren H, Li J, Sun B, Lu D, Li S, et al. Multifunctional ZnFe₂O₄-based antibiotic cross-linked nanoplatform for magnetically targeted treatment of microbial biofilms. *ACS Applied Nano Materials*. 2023;6(3):2141-50.
3. Soufi A, Hajjaoui H, Elmoubarki R, Abdennouri M, Qourzal S, Barka N. Spinel ferrites nanoparticles: Synthesis methods and application in heterogeneous Fenton oxidation of organic pollutants – A review. *Applied Surface Science Advances*. 2021;6:100145.
4. Zhang Z, Yao G, Zhang X, Ma J, Lin H. Synthesis and characterization of nickel ferrite nanoparticles via planetary ball milling assisted solid-state reaction. *Ceramics international*. 2015;41:4523-4530.
5. Phuruangrat A, Maisang W, Phonkhokkong T, Thongtem S, Thongtem T. Superparamagnetic and ferromagnetic behavior of ZnFe₂O₄ nanoparticles synthesized by microwave-assisted hydrothermal method. *Russian Journal of Physical Chemistry A*. 2017;91(5):951-6.
6. Kumar M, Singh Dosanjh H, Sonika, Singh J, Monir K, Singh H. Review on magnetic nanoferrites and their composites as alternatives in waste water treatment: synthesis, modifications and applications. *Environmental Science: Water Research & Technology*. 2020;6(3):491-514.
7. Reddy DHK, Yun YS. Spinel ferrite magnetic adsorbents: alternative future materials for water purification, *Coord. Chem Rev*. 2016;315:90-111.
8. Wang J, Zhang K, Zhu Y. Synthesis of SiO₂-coated ZnMnFe₂O₄ nanospheres with improved magnetic

- properties. Journal of Nanoscience and Nanotechnology. 2005;5(5):772-5.
9. Granone LI, Ulpe AC, Robben L, Klimke S, Jahns M, Renz F, et al. Effect of the degree of inversion on optical properties of spinel $ZnFe_2O_4$. Physical Chemistry Chemical Physics. 2018;20(44):28267-78.
 10. Li Y, Zhao J, Han J. Self propagation high temperature synthesis and magnetic properties of $Ni_{0.35}Zn_{0.65}Fe_2O_4$ powders. Bulletin of Materials Science. 2002;25(4):263-6.
 11. Linh NLM, Giang HTB, Thang LQ, Tien TD, Thu NTA, Duong T, et al. The Benzylation of *p*-xylene using $ZnFe_2O_4$ nanoparticles as heterogeneous catalyst. Journal of Nanomaterials. 2022;2022(1):6490334.
 12. Wang DK, Varanasi S, Fredericks PM, Hill DJT, Symons AL, Whittaker AK, et al. FT-IR characterization and hydrolysis of PLA-PEG-PLA based copolyester hydrogels with short PLA segments and a cytocompatibility study. Journal of Polymer Science Part A: Polymer Chemistry. 2013;51(24):5163-76.
 13. Bahtiar S, Taufiq A, Sunaryono, Hidayat A, Hidayat N, Diantoro M, et al. Synthesis, Investigation on Structural and Magnetic Behaviors of Spinel M-Ferrite [M = Fe; Zn; Mn] Nanoparticles from Iron Sand. IOP Conference Series: Materials Science and Engineering. 2017;202(1):012052.